

# Suppression of thermal vorticity as an indicator of QCD critical point

Sushant K. Singh<sup>1,2,\*</sup> and Jan-e Alam<sup>1,2</sup>

<sup>1</sup>Variable Energy Cyclotron Centre, 1/AF, Bidhan Nagar, Kolkata, India

<sup>2</sup>HBNI, Training School Complex, Anushakti Nagar, Mumbai 400085, India

(Dated: November 1, 2021)

We study the impact of QCD critical point on the spin polarization of  $\Lambda$ -hyperon generated by the thermal vorticity in viscous quark gluon plasma. The equations for the relativistic causal hydrodynamics have been solved numerically in (3+1) dimensions to evaluate the thermal vorticity. The effects of the critical point has been incorporated through the equation of state and the scaling behaviour of the transport coefficients. A significant reduction in the polarization has been found as the critical point is approached in comparison to the case when the critical point is absent.

PACS numbers:

The numerical simulation of QCD on lattice and QCD based effective field models at non-zero temperature ( $T$ ) and baryonic chemical potential ( $\mu$ ) reveals a rich and complex structure of QCD phase diagram [1–7]. While at high  $T$  and low  $\mu$  ( $\rightarrow 0$ ) the quark-hadron transition is a cross-over, at low  $T$  and high  $\mu$  the transition is of first order in nature. Therefore, it is expected that between the cross over and the first order transition there exists a point in the  $\mu - T$  plane, the Critical End Point or simply Critical Point (CP) where the first order transition ends and crossover begins [8]. The existence and the location of CP is not yet known from the first principle [9], however, phenomenological studies indicate the existence of the CP [10]. The experimental search for the CP through the system formed in collisions of nuclei at relativistic energies is one of the outstanding problem. At present the general consensus is that the collisions of nuclei at the top Relativistic Heavy Ion Collider (RHIC) and Large Hadron Collider (LHC) energies result in the formation of Quark Gluon Plasma (QGP) with small  $\mu$  and high  $T$  which reverts to hadronic phase via a cross over. The ongoing Beam Energy Scan (BES)- II program at RHIC and the upcoming Compressed Baryonic Matter (CBM) experiment at Facility for Anti-proton and Ion Research (FAIR) and Nuclotron based Ion Collider Facility (NICA) at the Joint Institute for Nuclear Research (JINR) are planned to create thermal system of quarks and gluons with different  $\mu$  and  $T$  by varying the collision energies to explore the region close to CP of the QCD phase diagram. Relativistic hydrodynamics has been used to describe the space-time evolution of QGP and explain various experimental data quite successfully. One such crucial observable is the global polarization of  $\Lambda$ -hyperon [11] generated by the thermal vorticity during the hydrodynamic evolution of the QGP.

The magnetization of uncharged objects induced by mechanical rotation, called Barnett effect [12] and its inverse, that is, the rotation generated by varying magnetization, called the Einstein-de Haas effect [13] originate due to the conversion between spin ( $S$ ) and orbital angular momentum ( $L$ ) via spin-orbit coupling constrained by

the conservation of total angular momentum  $\vec{J}(= \vec{L} + \vec{S})$ . Similar kind of coupling between  $L$  and  $S$  in the system formed in relativistic heavy ion collision will lead to the spin polarization of particles. The initial angular momentum being imparted by the spectators in non-central collision of fast nuclei may compel the fireball of QGP to rotate and polarize the particles [14]. Since there are no external torques acting on the fireball the total angular momentum will be conserved throughout the space-time evolution of the fireball. The total angular momentum has two components due to (i) the rotation of the fireball about its axis ( $y$ -axis if  $xz$ -plane is the reaction plane) and (ii) the spinning of fluid elements in the respective local rest frames (LRFs). Vorticity describes the local rotation of fluid elements and hence is related to the spinning of fluid elements in respective LRFs. The coupling of fluid vorticity and quantum mechanical spin has been experimentally demonstrated for the first time [15]. The fluid vorticity generated by viscosity of QGP will show similar coupling leading to polarization ( $P$ ) of spin 1/2 particles.

The presence of critical point in the equation of state affects the expansion of the system due to the suppression of the sound mode and divergence of some of the transport coefficients [16]. This will affect the evolution of local vorticity and hence the  $\Lambda$ -polarization. Apart from polarization the effects of CP on the separation of baryon and anti-baryon due to chiral vortical effects is another interesting facet [17]. In this work the impact of the CP on the polarization of  $\Lambda$  due to the vorticity-spin coupling is investigated and shown that as the critical point is approached the local vorticity and hence the polarization effect is suppressed.

Here we use natural units  $c = \hbar = k_B = 1$  where  $c$  is the speed of light in vacuum,  $h = 2\pi\hbar$  is the Planck's constant and  $k_B$  is the Boltzmann's constant. The signature metric for flat space time is taken as  $g_{\mu\nu} = \text{diag}(1, -1, -1, -1)$ .

We have developed a numerical code in FORTRAN to solve (3+1)-dimensional viscous relativistic causal hydrodynamics using the algorithm detailed in Ref. [18].

The code contains the effect CP through the Equation of State (EoS) and the scaling behaviour of the transport coefficients. The results from the code have been tested against known analytical [19] and numerical results available in the literature for system away from CP.

The relevant relativistic hydrodynamic equations solved are:

$$\begin{aligned}\partial_\mu T^{\mu\nu} &= 0, \\ \partial_\mu N^\mu &= 0,\end{aligned}\quad (1)$$

where  $T^{\mu\nu}$  is the energy-momentum tensor and  $N^\mu$  is the net-baryon number current. We choose to work in the Landau frame of reference where the  $T^{\mu\nu}$  and  $N^\mu$  take the following form:

$$T^{\mu\nu} = \varepsilon u^\mu u^\nu - (p + \Pi)\Delta^{\mu\nu} + \pi^{\mu\nu}, \quad (2)$$

$$N^\mu = n_B u^\mu + V^\mu, \quad (3)$$

where  $\Pi$  is the bulk pressure,  $\pi^{\mu\nu}$  is the shear-stress tensor which is symmetric, traceless and orthogonal to  $u^\mu$ ,  $V^\mu (= 0, \text{ here})$  is the baryon diffusion 4-current and  $\Delta^{\mu\nu} = g^{\mu\nu} - u^\mu u^\nu$ . The viscous terms obey the following evolution equations,

$$u^\alpha \partial_\alpha \Pi = -\frac{\Pi - \Pi_{NS}}{\tau_\Pi} - \frac{4}{3}\Pi \partial_\alpha u^\alpha, \quad (4)$$

$$\langle u^\alpha \partial_\alpha \pi^{\mu\nu} \rangle = -\frac{\pi^{\mu\nu} - \pi_{NS}^{\mu\nu}}{\tau_\pi} - \frac{4}{3}\pi^{\mu\nu} \partial_\alpha u^\alpha, \quad (5)$$

where  $\langle \cdot \rangle$  is defined as,

$$\langle A^{\mu\nu} \rangle = \left( \frac{1}{2}\Delta_\alpha^\mu \Delta_\beta^\nu + \frac{1}{2}\Delta_\alpha^\nu \Delta_\beta^\mu - \frac{1}{3}\Delta^{\mu\nu} \Delta_{\alpha\beta} \right) A^{\alpha\beta},$$

and  $\Pi_{NS}$ ,  $\pi_{NS}^{\mu\nu}$  are the Navier-Stokes limit of  $\Pi$  and  $\pi^{\mu\nu}$  respectively and are given by

$$\Pi_{NS} = -\zeta\theta \quad , \quad \pi_{NS}^{\mu\nu} = 2\eta \langle \partial^\alpha u^\beta \rangle. \quad (6)$$

The coefficients of shear ( $\eta$ ) and bulk ( $\zeta$ ) viscosities are positive, *i.e.*  $\eta, \zeta > 0$ .

We need to solve the hydrodynamical equations for specific initial conditions and EoS to evaluate the polarization of the  $\Lambda$  via thermal vorticity at the freeze-out surface where hydrodynamic evolution ceases. The hydrodynamic equations are solved in  $(\tau, x, y, \eta_s)$  coordinates where  $\tau = \sqrt{t^2 - z^2}$  and  $\eta_s = \tanh^{-1}(z/t)$ . The space-time evolution begins at  $\tau_0$ . For lower energies the initial time,  $\tau_0$  is taken as the time required by the nuclei to pass through one other ( $\sim \frac{2R}{\gamma_z v_z}$ ) and for higher energies ( $\sqrt{s_{NN}} \geq 24$  GeV),  $\tau_0 = 1$  fm as shown in Table I. The initial energy density profile at  $\tau_0$  is taken as:

$$\varepsilon(x, y, \eta_s; \tau_0) = e(x, y) f(\eta_s). \quad (7)$$

A symmetric rapidity profile,  $f(\eta_s)$ , with the local energy-momentum conservation puts a constraint on

$e(x, y)$  as shown in Ref. [20]. The energy deposited in the transverse plane,  $e(x, y)$  depends on the number of wounded nucleons per unit area,  $n_A^W$  and  $n_B^W$  of nuclei  $A$  and  $B$  respectively which are calculated by using the optical Glauber model as:

$$n_{A,B}^{(W)} = T_{A,B} \left[ 1 - \left( 1 - \frac{\sigma_{NN}^{\text{in}} T_{B,A}}{N_{B,A}} \right)^{N_{B,A}} \right]. \quad (8)$$

where  $N_A$  and  $N_B$  are the total number of nucleons in  $A$  and  $B$  respectively. The nucleon-nucleon inelastic cross-section,  $\sigma_{NN}^{\text{in}}(\sqrt{s_{NN}})$  has been estimated by using the parametrization given in Refs. [21, 22]. The thickness functions  $T_A(x, y)$  and  $T_B(x, y)$  are calculated as follows:

$$T_{A,B}(x, y) = \int_{-\infty}^{\infty} \rho_{A,B}(x, y, z') dz', \quad (9)$$

where  $\rho_{A,B}(x, y, z)$  is the nuclear density profile taken as

$$\rho_{A,B}(x, y, z) = \frac{\rho_0}{1 + e^{\frac{r-R(\theta)}{\delta}}}, \quad (10)$$

where  $\rho_0$  is chosen such that:  $\int \rho_i(\vec{r}) d^3\vec{r} = N_i$ ,  $i = A, B$  and  $R(\theta)$  takes into account the deformation of the nucleus as:  $R(\theta) = R[1 + \beta_2 Y_{2,0}(\theta) + \beta_4 Y_{4,0}(\theta)]$  where  $Y_{l,m}(\theta, \phi)$  are the spherical harmonics. In the present case we take  $R(\theta) = R = 6.37$  fm for collisions of spherical Au+Au nucleus. The function  $e(x, y)$  appearing above is related to the thickness function as;  $e(x, y) \propto (T_A^2 + T_B^2 + 2T_A T_B \cosh(2y_{beam}))$ , where  $y_{beam} = \text{arccosh}(\sqrt{s_{NN}}/2)$ . The initial velocity profile is taken as:

$$u^\mu(x, y, \eta_s; \tau_0) = (\cosh(\eta_s), 0, 0, \sinh(\eta_s)), \quad (11)$$

The initial density profiles for energy and net baryon number have been computed with the parameters of [20] and then curve fitting method has been used to obtain the same at intermediate energies. In the present work the value of the impact parameter ( $b$ ) is taken as  $b = 5$  fm.

TABLE I: Values of  $\tau_0$  used at different colliding energies

$\sqrt{s_{NN}}$ (GeV)	14	16	18	20	24	28	36	62.4	200
$\tau_0$ (fm)	1.7	1.5	1.3	1.2	1.0	1.0	1.0	1.0	1.0

The EoS [23] employed here to solve the hydrodynamic equations reproduces the lattice QCD results at zero chemical potential. The transport coefficients are expected to diverge near the critical point following a scaling behavior [24]:

$$\zeta \sim \xi^3 \quad , \quad \eta \sim \xi^{0.05}.$$

where  $\xi(\mu, T)$  is the equilibrium correlation length. The extent of the critical domain in the  $\mu - T$  plane is determined by the condition:  $\xi(\mu, T) = \xi_0$ , where  $\xi_0$  is taken

as 1.75 fm. The possibility of divergent behaviour is incorporated in the present study through the following expressions of the transport coefficients [24]

$$\zeta = \zeta_0 \left( \frac{\xi}{\xi_0} \right)^3, \quad \eta = \eta_0 \left( \frac{\xi}{\xi_0} \right)^{0.05} \quad (12)$$

Outside the critical region the values of the shear and bulk viscosities denoted by  $\eta_0$ ,  $\zeta_0$  respectively are chosen as [25, 26]:

$$\eta_0(\mu_B, T) = 0.08 \left( \frac{\varepsilon + p}{T} \right), \quad \zeta_0(\mu_B, T) = 15 \eta_0 \left( \frac{1}{3} - c_s^2 \right)^2$$

The behaviour of the relaxation times appeared in Eqs.(4) and (5) are parametrized as:

$$\tau_\pi = \tau_\pi^0 \left( \frac{\xi}{\xi_0} \right)^{0.05}, \quad \tau_\Pi = \tau_\Pi^0 \left( \frac{\xi}{\xi_0} \right)^3. \quad (13)$$

where  $\tau_\pi^0$  and  $\tau_\Pi^0$  are the relaxation times outside the critical region which are given by [26],

$$\frac{\tau_\pi^0}{5} = \tau_\Pi^0 = \frac{C_\eta}{T}.$$

with  $C_\eta = 0.08$ .

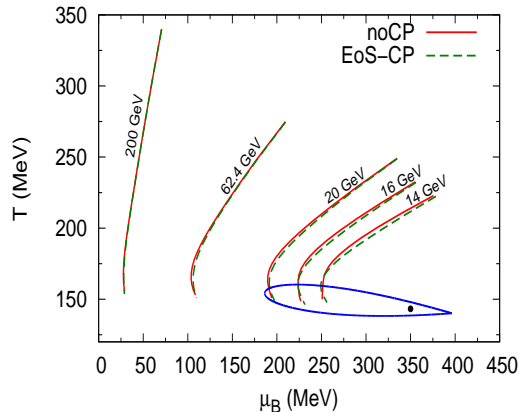


FIG. 1: Trajectories traced by the center of the fireball *i.e.*  $x = y = \eta_s = 0$  in the  $\mu - T$  plane for different colliding energies. The critical point is indicated by solid black dot at  $(\mu_c, T_c) = (350, 143.2)$  MeV.

The critical region and the trajectories traced by the center of the fireball in the  $(\mu - T)$  plane at different colliding energies are shown in Fig. 1. The black dot indicates the location of the CP at  $(\mu_c, T_c) = (350, 143.2)$  MeV. The hydrodynamic evolution curves have been calculated by solving the hydrodynamic equations with and without the effects of CP for initial conditions discussed before and stop the evolution at the freeze-out surface defined by  $\varepsilon = 0.3 \text{ GeV}/\text{fm}^3$ . The CORNELIUS code [27] has been used to find the constant  $\varepsilon = 0.3 \text{ GeV}/\text{fm}^3$  surface within a computational

(fluid) cell. The trajectories for  $\sqrt{s_{NN}} = 14 \text{ GeV}$ , 16 GeV and 20 GeV pass through the critical domain (shown by the closed contour in Fig. 1) defined by the relation,  $\xi(\mu, T) = 1.75 \text{ fm}$  and those for higher  $\sqrt{s_{NN}}$  remain outside the critical domain. As a next step we evaluate the thermal vorticity and subsequently the polarization of  $\Lambda$  for system evolving along trajectories which are passing through both inside and outside the critical domain.

The thermal vorticity is a measure of microscopic rotation at any space-time point of the fluid which is given by [28, 29]:

$$\varpi_{\mu\nu} = \frac{1}{2} [\partial_\nu \beta_\mu - \partial_\mu \beta_\nu] \quad (14)$$

where  $\beta_\mu = u_\mu/T$ . The time evolution of the  $x\eta$  component of the vorticity averaged over the  $(x, y, \eta)$  coordinates weighted by the energy density with and without the effects of CP have been shown in Fig. 2. The system has zero vorticity initially. However, as the system evolves the non-zero vorticity is created by shear viscous effects. The evolution of the vorticity is affected by several factors. While the hydrodynamic expansion redistribute the vortices, the viscous coefficients are responsible for diffusing it. In addition to these, the vortex stretching and the baroclinic torque can enhance the vorticity [30]. The CP directly affects the expansion because of the absorption of sound wave as the system approach CP and the diverging nature of viscous coefficient near CP will enhance the diffusion leading to the reduction in the absolute value of the vorticity as seen in Fig. 2. As the evolution trajectory for  $\sqrt{s_{NN}} = 62.4 \text{ GeV}$  remain outside the critical domain the results with and without the CP overlap.

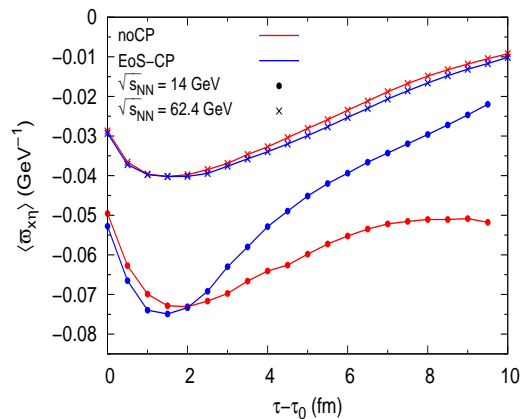


FIG. 2: Time evolution of  $x\eta$ -component of thermal vorticity for  $\sqrt{s_{NN}} = 14 \text{ GeV}$  and 62.4 GeV.

The local thermal vorticity and hence the  $\Lambda$ -hyperon polarization is calculated at this point using the following expression for mean spin vector of a spin-1/2 particle

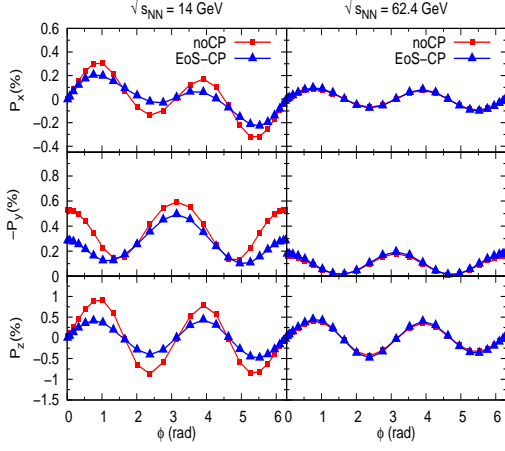


FIG. 3:  $x$ ,  $y$  and  $z$  components of  $\Lambda$ -polarization are plotted respectively in the upper, middle and the lower panels as a function of azimuthal angle in momentum space for  $\sqrt{s_{NN}} = 14\text{GeV}$  and  $62.4\text{ GeV}$ .

with momentum  $p$  [31] as,

$$S^\mu(x, p) = -\frac{1}{8m}(1 - n_F)\epsilon^{\mu\nu\rho\sigma}p_\nu\varpi_{\rho\sigma}(x) + O(\varpi)^2$$

where  $m$  is the mass of the particle,  $\epsilon^{\mu\nu\rho\sigma}$  is the Levi-Civita tensor and  $n_F$  is the Fermi-Dirac distribution. Since the mass of the  $\Lambda$  is much larger than the temperature range being considered in this study we assume that  $1 - n_F \approx 1$  and  $n_F \approx n_B$  where  $n_B$  is the Boltzmann distribution. Consequently the expression for the mean spin vector becomes

$$S^\mu(x, p) = \frac{1}{8m}\epsilon^{\mu\nu\rho\sigma}p_\nu\partial_\rho\beta_\sigma$$

In the rest frame of the particle, the spin vector is  $S^{*\mu} = (0, \mathbf{S}^*)$ . The corresponding quantities in the rest frame of the particle is obtained by using the Lorentz transformation as:

$$\mathbf{S}^* = \mathbf{S} - \frac{\mathbf{p}\cdot\mathbf{S}}{E(E+m)}\mathbf{p}$$

The mean spin averaged over the surface  $\Sigma$  is then given by,

$$S^\mu(p) = \frac{\int d\Sigma_\lambda p^\lambda e^{-\beta(p\cdot u - \mu_B)} S^\mu(x, p)}{\int d\Sigma_\lambda p^\lambda e^{-\beta(p\cdot u - \mu_B)}} \quad (15)$$

The net spin is obtained by integrating over azimuthal angle, rapidity and transverse momentum ( $|y| < 1$ ) and transverse momentum ( $0 < p_T < 3\text{ GeV}$ ). Finally the spin polarization of  $\Lambda$  is given by,

$$\mathbf{P} = 2\mathbf{S}^*$$

Different components of the polarization,  $P_x$ ,  $P_y$  and  $P_z$  have been calculated at the freeze-out surface with

and without the effects of CP on the solutions of hydrodynamic equations. The variations of  $P_x$ ,  $P_y$  and  $P_z$  with azimuthal angle ( $\phi$ ) have been depicted in Fig. 3 at  $\sqrt{s_{NN}} = 14\text{ GeV}$  and  $62.4\text{ GeV}$  with and without the effects of CP. We observe that for the chosen coordinate system ( $xz$  as the reaction plane and  $y$ -axis is the axis of rotation) the magnitude of the Cartesian components of the polarization are similar. A systematic suppression of the polarization is observed at  $\sqrt{s_{NN}} = 14\text{ GeV}$  which originates from the enhanced diffusivity of the vorticity caused by the large viscosity near the CP. The polarizations overlap at  $\sqrt{s_{NN}} = 62.4\text{ GeV}$  which is obvious as the trajectory for this collision energy is outside the critical domain (Fig. 1).

The change in  $P_y$  with  $y$  (rapidity) is displayed in Fig. 4 which again shows a clear suppression of polarization due to the presence of CP at  $\sqrt{s_{NN}} = 14\text{ GeV}$ . The diverging nature of the viscous coefficients near the CP plays the most dominant role in reducing the vorticity and subsequently the polarization. At  $\sqrt{s_{NN}} = 62.4\text{ GeV}$  the  $P_y$  with and without CP is identical as expected. It is very interesting to note that the CP not only changes the polarization around mid-rapidity quantitatively but also introduce strong qualitative changes in the shape of the curve. Such a change in the spin polarization will be an indicator of the existence of CP.

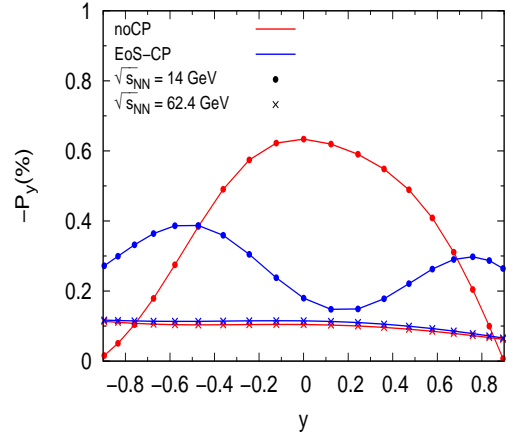


FIG. 4:  $y$ -component of  $\Lambda$ -polarization plotted as a function of momentum rapidity for  $\sqrt{s_{NN}} = 14\text{ and }62.4\text{ GeV}$ .

Finally, on integration over  $p_T$ ,  $\phi$  and  $y$  the polarization,  $P_y$  is obtained as a function of  $\sqrt{s_{NN}}$ . The suppression of polarization is conspicuous for the trajectories passing through the critical domain at lower  $\sqrt{s_{NN}}$  (Fig. 5). We have taken the initial angular momentum of the fireball as zero resulting in smaller polarization compared to experimental value [11]. Inclusion of initial angular momentum through the non-zero initial value of the velocity profile [28] will enhance the magnitude of  $-P_y$ , however, the difference in the polarization observed here with and without CP will still persist. The slope of

the curve without CP at lower  $\sqrt{s_{NN}}$  is much steeper than the one with CP. Therefore, the detection in the reduction of the polarization will shed light on the existence of CP in the system formed in relativistic heavy ion collisions.

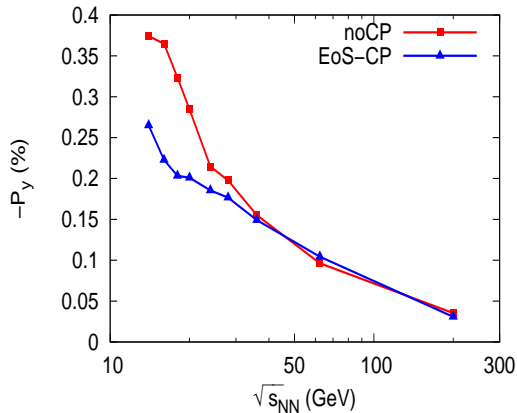


FIG. 5: Polarization of  $\Lambda$ -hyperon plotted as a function of  $\sqrt{s_{NN}}$ .

We have solved the equations for viscous causal hydrodynamics in (3+1) dimensions for evolving quark gluon plasma for different initial conditions corresponding to different  $\sqrt{s_{NN}}$ . We have taken into account the effects of CP through the EoS and scaling behaviour of the shear and bulk viscosities. The thermal vorticity for different colliding energies have then been estimated and found to be suppressed as the CP is approached due to the diverging nature of viscous coefficients which facilitate the diffusion of vorticity. The local vorticity of the fluid couples with the quantum mechanical spin of the particles and polarize it along the direction of the vorticity. We have evaluated the spin polarization of  $\Lambda$ -hyperon with and without the effects of CP. We find a strong change in the spin polarization around mid-rapidity as the system approach the CP. It is also observed that the spin polarization is suppressed in system which admits CP. These observations will be useful in detecting the CP experimentally.

Some comments on the application of hydrodynamics near the CP is in order here. Since hydrodynamics is based on the assumption of local thermal equilibrium (LTE), if a few modes do not relax faster compared to the timescale of changes in slow/conserved variables, then LTE cannot be maintained and consequently hydrodynamics breaks down. That is, in the neighborhood of the CP, if the rate of relaxation of the modes connected to the critical fluctuation are comparable to (or less than) the hydrodynamic modes associated with the conserved charges then hydrodynamics becomes invalid. In such a situation the validity of the hydrodynamics can be extended by adding a slow non-hydrodynamic modes

connected to the relaxation rate of the critical fluctuation (see [32] and [33] for details). Namely, one more scalar variable (representing the slow mode) is introduced in addition to the other hydrodynamic variables (energy density, charge density and fluid velocity). to describe the evolution of the system near the CP. In a simple picture describing the evolution of a system with boost invariance it has been explicitly shown that the modes associated with the scalar variable lags behind the hydrodynamic modes resulting in back reactions on the hydrodynamic variables [34]. Further, it has been demonstrated in Ref. [34] that the back reaction has negligible effects on the hydrodynamic variables. In view of this the results presented in this work can be considered as reasonable. Moreover, we may also recall that if a system is not too close to CP then hydrodynamics can still be applied in a domain around the CP [35].

- 
- \* Correspondence email address: sushant7557@gmail.com
- [1] A. Bazavov, F. Karsch, S. Mukherjee and P. Petreczky (USQCD Collaboration), arXiv:1904.09951 [hep-lat].
  - [2] Z. Fodor and S. Katz, JHEP **03**, 014 (2002).
  - [3] M. Asakawa and K. Yazaki, Nucl. Phys. A **504**, 668 (1989).
  - [4] A. M. Halasz, A. Jackson, R. Shrock, M. A. Stephanov and J. Verbaarschot, Phys. Rev. D **58**, 096007 (1998).
  - [5] P. de Forcrand and O. Philipsen, Nucl. Phys. B **642**, 290 (2002).
  - [6] Y. Aoki, G. Endrodi, Z. Fodor, S. Katz and K. Szabo, Nature **443**, 675 (2006).
  - [7] G. Endrodi, Z. Fodor, S. Katz and K. Szabo, JHEP **04**, 001 (2011).
  - [8] Z. Fodor and S. Katz, JHEP **04**, 050 (2004).
  - [9] H. T. Ding, F. Karsch and S. Mukherjee, Int. J. Mod. Phys. E **24**, 1530007 (2015).
  - [10] M. A. Stephanov, K. Rajagopal and E. V. Shuryak, Phys. Rev. Lett. **81**, 4816 (1998).
  - [11] L. Adamczyk *et al.* (for STAR collaboration), Nature **548**, 63 (2017).
  - [12] S. J. Barnett, Phys. Rev. **6**, 239 (1915).
  - [13] A. Einstein and W. J. de-Haas, Ver. Dtsch. Ges. **17**, 152 (1915).
  - [14] Z. T. Liang and X. N. Wang, Phys. Rev. Lett. **94**, 102301 (2005); Z. T. Liang and X. N. Wang, Phys. Rev. Lett. **96**, 039901 (2005).
  - [15] R. Takahashi *et al.*, Nat. Phys. **12**, 52 (2016).
  - [16] Md Hasanujjaman, M. Rahaman, A. Bhattacharyya and J. Alam, Phys. Rev. C **102**, 034910 (2020).
  - [17] D. E. Kharzeev, J. Liao, S. A. Voloshin and G. Wang, Prog. Part. Nucl. Phys. **88**, 1 (2016).
  - [18] Iu. Karpenko *et al.*, Comput. Phys. Commun. **185** (2014) 3016–3027.
  - [19] S. S. Gubser, Phys. Rev. D **82**, 085027 (2010).
  - [20] C. Shen and S. Alzhirani, Phys. Rev. C **102**, 014909 (2020).
  - [21] J. Cudell *et al.* (COMPETE), Phys. Rev. Lett. **89**, 201801 (2002).
  - [22] B. Abelev *et al.* (ALICE Collaboration) Phys. Rev. C **88**,

- 044909 (2013).
- [23] P. Parotto *et al.*, Phys. Rev. C 101, 034901 (2020).
- [24] A. Monnai, S. Mukherjee and Y. Yin, Phys. Rev. C **95**, 034902 (2017).
- [25] G. S. Denicol, C. Gale, S. Jeon, A. Monnai, B. Schenke, and C. Shen, Phys. Rev. C **98**, 034916 (2018).
- [26] Denicol, G. S. and Jeon, S. and Gale, C., Phys. Rev. C **90**, 024912 (2014).
- [27] <https://link.springer.com/article/10.1140>
- [28] F. Becattini, *et al.*, Eur. Phys. J. C **75**, 406 (2015).
- [29] F. Becattini, Iu. Karpenko, M. A. Lisa, I. Upsal and S. A. Voloshin, Phys. Rev. C **95**, 054902 (2013); F. Becattini, L. P. Csernai and D. J. Wang, Phys. Rev. C **88**, 034905 (2013).
- [30] S. K. Singh *et al.*, to be published.
- [31] F. Becattini, V. Chandra, L. D. Zanna and E. Grossi, Ann. Phys. **338**, 32 (2013); R.-h. Feng, L.-g. Pang, Q. Wang and X. N. Wang, Phys. Rev. C **94**, 024904 (2016).
- [32] M. Stephanov and Y. Yin, Nucl. Phys. A **967**, 876 (2017).
- [33] M. Stephanov and Y. Yin, Phys. Rev. D **98**, 036006 (2018).
- [34] K. Rajagopal, G. W. Ridgway, R. Weller and Y Yin, Phys. Rev. D **102**, 094025 (2020).
- [35] H. E. Stanley, Introduction to phase transitions and critical phenomena, Oxford University Press, 1971.